Toxicology Research

PAPER

Cite this: *Toxicol. Res.*, 2015, **4**, 885

Toxicity mechanism of graphene oxide and nitrogen-doped graphene quantum dots in RBCs revealed by surface-enhanced infrared absorption spectroscopy†

Tiantian Wang,[a,b] Shoujun Zhu[c] and Xiue Jiang*[a]

Received 20th September 2014,
Accepted 19th January 2015

DOI: 10.1039/c4tx00138a

www.rsc.org/toxicology

The study of the toxic effects of nanoparticles on biological systems at the molecular level is critical in order to gain a greater understanding of the origin of nanotoxicity. Recently, numerous forms of graphene materials have been synthesized and extensively applied in biosensors and biomedicine, but their toxicity has not yet been studied to the same extend, in particular the toxicity mechanism. In this work, we systematically studied the toxic effects of two typical graphene forms, graphene oxide (GO) and nitrogen-doped graphene quantum dots (N-GQDs), on red blood cells (RBCs) by testing their hemolytic activity, observing the morphological changes and detecting the ATP content of RBCs after being exposed to the two nanomaterials. The toxicity mechanism was further revealed by investigating the structural changes of RBCs lipid by surface-enhanced infrared absorption spectroscopy using model membranes. A detailed analysis of the infrared spectra revealed that the adsorption of GO destroys the integrity of a membrane by extracting the lipid bilayer, resulting in hemolysis and aberrant forms. In contrast, N-GQDs just disturb the structure and conformation of the lipid, resulting in only aberrant cells. To date, this is the first experimental study which has revealed the toxicity mechanism of graphene materials in RBCs at the molecular level.

Introduction

With the booming development of nanotechnology in the past decades, there has been a rapid expansion in the types of engineered nanoparticles used in different areas of industry, technology, and medicine, where they have shown tremendous advantages. However, the nano size not only gives materials unique physicochemical properties which means that they behave very differently from the bulk forms of the same material, but their size also makes their potential health and environmental effects extremely difficult to predict. Therefore, a recent trend in nanotechnology has been the investigation of the interactions of nanomaterials with biological systems.[1] There is increasing concern as to whether and how nanomaterials are potentially toxic to biological systems.[2–7]

As a two-dimensional carbon sheet of single-atom thickness, graphene has received much attention due to its outstanding mechanical, thermal, chemical and optical properties.[8–11] Among the various graphene forms, graphene oxide (GO) contains multifunctional groups, such as carboxyl, epoxy, ketone, and hydroxyl groups, in its basal and edge planes,[12,13] which results in good water-solubility and an excellent capability for conjugating with biomolecules and metallic nanoparticles.[14,15] In this regard, GO has shown great potential for biological applications[16,17] including cancer cell detection,[14] *in situ* molecular probing in living cells,[15] immunoassays,[18] biosensing,[19] cellular imaging,[20] and drug delivery.[20,21] As novel kinds of quantum dots and graphene forms, graphene quantum dots (GQDs) prepared from GO have shown promising potential in photovoltaic devices, biosensing, and bioimaging because of their stable photoluminescence, high solubility, low toxicity, and good biocompatibility.[22,23] Owing to their ultrahigh specific surface area, GQDs can be easily modified, functionalized, and used for drug or gene delivery.[24–26]

Because of the widespread application of graphene and its derivatives in nanobiomedicine, their toxicity has attracted tremendous research interest.[3,27–31] It has been reported that GO can induce cellular oxidative stress at low concentration and thrombus in mouse, and can evoke a strong aggregatory

[a]*State Key Laboratory of Electroanalytical Chemistry, Changchun Institute of Applied Chemistry, Chinese Academy of Sciences, Changchun 130022, China. E-mail: jiangxiue@ciac.ac.cn; Fax: +86 431 85685653; Tel: +86 431 85262426*
[b]*Graduate University of Chinese Academy of Sciences, Beijing 100049, China*
[c]*State Key Laboratory of Supramolecular Structure and Materials, College of Chemistry, Jilin University, Changchun, 130012, China*

† Electronic supplementary information (ESI) available: The AFM images of GO and N-GQDs. The hemolysis percent change with exposure time. The time-dependent SEIRA spectra of every step. See DOI: 10.1039/c4tx00138a

response in human platelets.[3,29] The oxygen content of graphene sheets has a strong impact on the toxicological response to RBCs,[27] and the toxicity of GO is also size-dependent.[12,31] In comparison with GO, the toxicity of GQDs has not yet been studied to the same extent. Most of the studies have estimated the biocompatibility of GQDs by means of simple methods, such as MTT assay.[32–34] As far as we know, only a few reports have systematically studied the *in vitro* and *in vivo* toxicity of GQDs, including their blood biocompatibility, *in vivo* biodistribution, cell viability, proliferation, metabolic activity, and their influence on tissues and organs.[28,35–37] Only one group has systematically evaluated the toxic effect of N-GQDs in an *in vivo* assay system using *C. elegans*.[38] All the results have proved that GQDs possess no obvious *in vitro* and *in vivo* toxicity. Although we have gained some insight into the toxic effects of graphene derivatives, the present conclusions were mostly drawn on the basis of cellular viability investigation, nanoparticle-induced morphological changes of the exposed cells, and some harmful results, such as thrombus and hemolysis. The underlying molecular mechanism remains unknown. Actually, cytotoxicity is initiated by the nonspecific adhesion of nanoparticles to the cell membranes. It is the discovery of the damage caused by carbon nanoparticles to cell membranes that has attracted people's attention to the nanotoxicity.[39] Therefore, understanding how nanoparticles interact with cell membranes is the first important step towards gaining insight into the underlying molecular mechanism of how nanoparticles induce cytotoxicity. In this regard, Zhou and co-workers have made the first step.[40] By using molecular dynamic simulations, they revealed atomic details about the interactions between graphene nanosheets and lipid molecules. They found that graphene nanosheets can penetrate into and extract phospholipids from the cell membranes.[40] However, experimental knowledge about the molecular mechanism of the cytotoxicity is still limited, and the simulation results require experimental support.

Surface-enhanced infrared absorption spectroscopy (SEIRAS) is a strictly surface sensitive technique that exploits the electromagnetic properties of nanostructured metal films to enhance the vibrational bands of adsorbed monolayers by a factor of 10–1000.[41,42] The resulting enrichment of sample along the solid surface reduces the content of water, and enables SEIRAS to investigate biological samples in aqueous environments, thereby overcoming the limits of the traditionally used attenuated total refection Fourier transform infrared (ATR-FTIR) spectroscopy, in which water represents a major obstacle.[43–45] In addition, this property also enables the biological samples–solvent interaction to be investigated to study the changes occuring in the microenvironment around biological samples. In a biomimetic system, SEIRAS can monitor the formation of a planar lipid bilayer and the adsorption of proteins or nanoparticles onto the bilayer *in situ* and in real-time.[42,46,47] SEIRA difference spectroscopy can finely reveal some minor structural changes of proteins[48–50] or lipids[42] upon electron and proton transfer or nanoparticles adsorption, providing a reliable experimental basis for further investigation and analysis.

In this work, we evaluated the toxicity of GO and N-GQDs using RBCs as model cells, and studied the toxicity mechanism employing SEIRAS to detect the GO and GQDs-induced structural changes of model membranes prepared on solid supports with lipid compositions identical to those of the inner and outer leaflet of RBC membranes. To some extent, our work will be significant for the design of graphene materials for safer and efficient biomedical applications.

Results and discussion

Synthesis and characterization of GO and GQDs

High yields of GO were synthesized by a modified Hummer's method,[51,52] and N-GQDs were sequentially prepared from GO by a one-step solvothermal route.[23] The morphologies of the as-prepared GO and N-GQDs were observed by TEM as shown in Fig. 1A and B, respectively. The GO sheet is flat and smooth with a few folds, and the size ranges from several hundred nanometers to several micrometers (Fig. 1A). However, the N-GQDs are uniform to a certain extent. The average size is about 5.1 nm as shown in the size histogram in the inset of Fig. 1B. AFM images proved that the height of GO is only 0.887 nm, suggesting a single-layer GO whereas the average height of N-GQDs is about 1.35 nm (Fig. S1†). Fig. 1C and D show the XPS scan spectra. It can be seen that the GO consists mainly of O and C. In the case of N-GQDs, in addition to O and C, there is a distinct peak attributed to N element in the spectrum, suggesting the participation of DMF as a weak reducing agent in

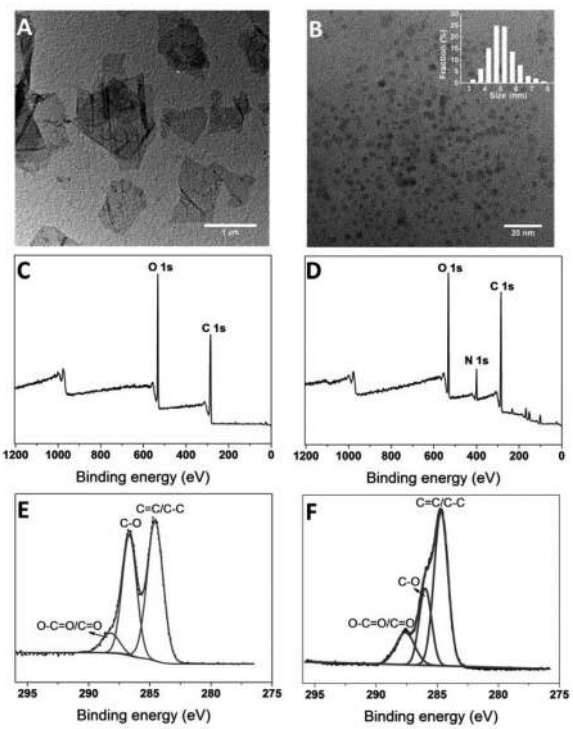

Fig. 1 TEM of GO (A) and N-GQDs (B) and their corresponding XPS spectra (C, D). The C1s XPS spectra of GO (E) and N-GQDs (F) were decomposed. Inset of (B) represents the size distribution of N-GQDs.

the preparation of N-GQDs.[23] Fig. 1E shows the high resolution C1s spectrum of GO fitted by three components. The binding peak at 284.6 eV is attributed to C═C/C–C in aromatic rings, the peak centered at 286.7 eV is assigned to C–O and the binding peak at 288.2 eV is due to C═O/O–C═O.[53,54] The content of the non-oxygenated C is about 49.37%, and that of the oxygenated C is about 50.63%. The high resolution C1s spectrum of N-GQDs was also fitted by three components as shown in Fig. 1F: C═C/C–C (284.7 eV), C–O (286.0 eV) and C═O (287.6 eV).[53–55] The percentage of non-oxygenated C increased to 58.07% in comparison to GO, and that of the oxygenated C decreased to 41.93% simultaneously, suggesting that some oxygen functional groups were lost during the preparation.

In vitro hemolytic activity of GO and N-GQDs

The application of nanomaterials in biomedicine always involves the intravenous injection of these materials. The injected nanomaterials finally reach the bloodstream and interact with RBCs. Therefore, evaluating the hemolytic activity of nanomaterials towards RBCs is very important and necessary for studying the nanotoxicity. Here, we firstly observed the hemolytic activity of N-GQDs and GO. Photographs of RBCs after exposure to N-GQDs and GO at different concentrations are shown in Fig. 2A. When the RBCs were treated with N-GQDs, no free hemoglobin in the supernatant was visualized, even if the N-GQDs concentration was as high as 200 μg mL^{-1}. However, when the RBCs were treated with GO, the color of the supernatant became redder with an increase of GO concentration, indicating that more and more hemoglobin was released from the RBCs. Furthermore, we evaluated the hemolytic activity of GO and N-GQDs by measuring the absorbance of the released hemoglobin using a UV-visible spectrometer and calculating the hemolysis percentage of the RBCs. As shown in Fig. 2B, the GO-induced hemolysis percent increases linearly with an increase of GO concentration until the concentration reaches 50 μg mL^{-1}. Above this concentration, the hemolysis gently increases to a constant. In contrast, N-GQDs did not induce any hemolysis even at high concentration. The color of the supernatant and the calculated hemolysis percent are similar to those in the negative control, indicating the low hemolytic activity of N-GQDs. We also studied the hemolysis percent change with exposure time at a concentration of 50 μg mL^{-1} (Fig. S2†). The results suggest that GO will induce more serious hemolysis, whereas N-GQDs will not induce obvious hemolysis within 7 h, which also indicates the low hemolytic activity of N-GQDs.

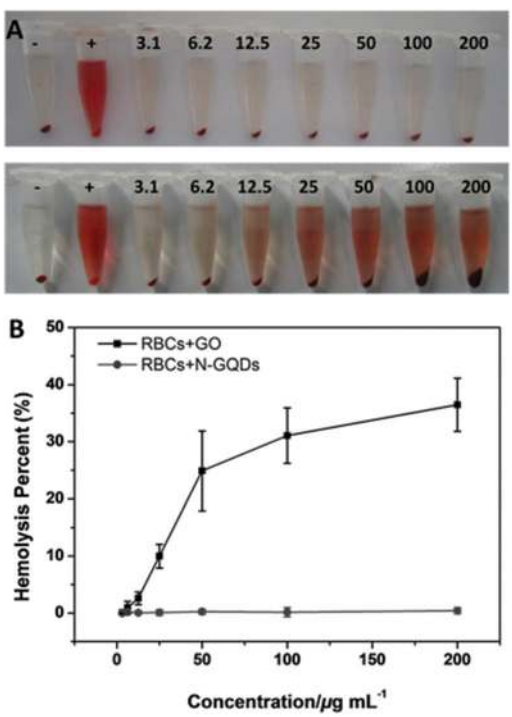

Fig. 2 (A) Photographs of RBCs after 3 h exposure to N-GQDs (upper) and GO (lower) at different concentrations (3.1 to 200 μg mL^{-1}). (+) and (–) symbols represent positive and negative control samples, respectively, which were prepared by mixing 0.2 mL of RBCs suspension with 0.8 mL of water and PBS respectively. (B) Hemolysis percent of RBCs incubated with different concentrations of GO (black) and N-GQDs (gray) for 3 h at 37 °C.

Observation of morphological changes of RBCs by confocal microscopy

In addition to hemolysis, exposure of RBCs to extraneous materials might also induce morphological aberrant forms, such as swollen cells,[56] stomatocytes,[57] echinocytes,[56,57] and haemagglutination.[56] These morphologically aberrant forms are frequently symptomatic of various medical conditions.[56] In order to further understand the toxic effects of GO and N-GQDs on RBCs, we observed, by means of confocal microscopy, the morphologies of RBCs after treatment with 50 μg mL^{-1} of GO or N-GQDs as an example, as shown in Fig. 3. Compared with the normal RBCs, in the control

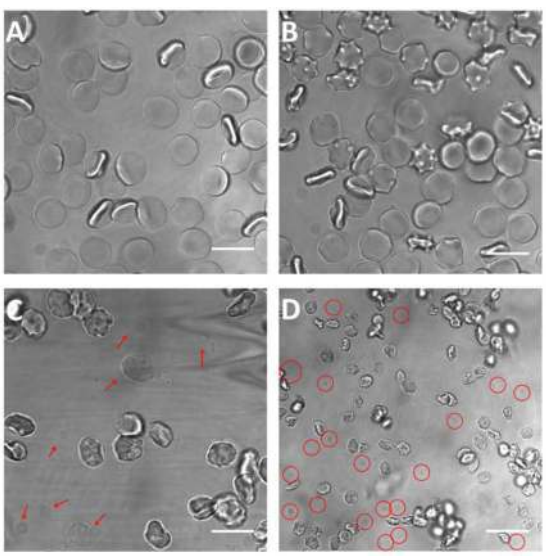

Fig. 3 Confocal images of RBCs incubated with (A) PBS (control), or (B) N-GQDs, and (C, D) GO at 50 μg mL^{-1} for 3 h at 37 °C. The arrow marks in (C) and circles in (D) indicate the ghost cells. Scale bars of (A–C) and (D) are 10 and 20 μm, respectively.

samples, which have a biconcave shape and a smooth membrane (Fig. 3A), treatment with N-GQDs resulted in about 50% echinocytes with numerous surface spikes (Fig. 3B). GQDs have been used in bioimaging and have been proved to be biocompatible by MTT assay, serum biochemical analysis and histological evaluation, *etc*.[23,28,35] However, their hemolytic activity and the corresponding morphological changes of RBCs have not been studied. The loss of the normal biconcave shape and the morphological variations in RBCs suggest that they exhibit a potential toxic effect. Compared with the control sample, RBCs treated with GO have both aberrant forms and ghost cells (Fig. 3C, arrows in red) due to the great hemolytic activity of GO. In the large-scale image presented in Fig. 3D, the proportion of ghost cells (circles in red) is shown to be below 40%, which is consistent with the hemolysis assay. The morphological changes of the RBCs suggests that N-GQDs and GO are potentially cytotoxic, and this needs further investigation for an in-depth understanding of the mechanism.

Detection of ATP content in RBCs

It is well known that adenosine triphosphate (ATP) is a universal energy source and an extracellular signaling mediator in many biological processes.[58] In RBCs, ATP also plays an important role in controlling the shape of RBCs.[57,59,60] When the content of ATP decreases below a certain level, RBCs lose their biconcave shape and transform into the crenated forms.[60] During the early stage of the transformation process echinocytes appear.[61,62] To explore the reason for the deformation of RBCs, we determined the ATP content in RBCs after incubation with GO or N-GQDs. As shown in Fig. 4, the ATP content in GO-treated RBCs decreases dramatically in comparison with that in the control RBCs, with only 20.7% being left, which might be partly due to the release of ATP accompanied by the release of hemoglobin when hemolysis occurred. The decrease of ATP may be one of the reasons for the appearance of aberrant forms as observed by confocal microscopy. In contrast, the amount of ATP in N-GQDs-treated RBCs remains at about 95% compared to that in the control RBCs, which is sufficient to maintain the normal biconcave disks of RBCs. So there should be other reasons for the N-GQDs-induced RBCs shape changes.

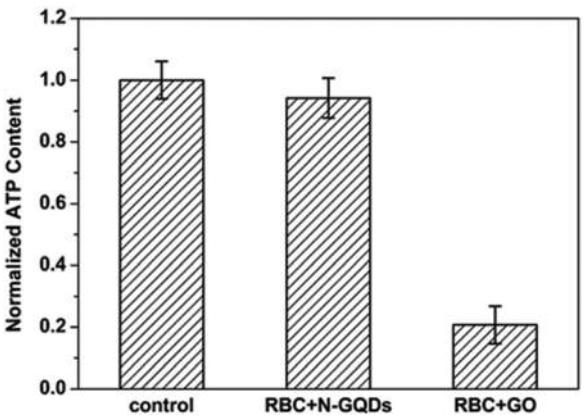

Fig. 4 The ATP percent of RBCs after treatment with PBS as control, or 50 μg mL^{-1} of N-GQDs and GO for 3 h at 37 °C. Mean ATP content was obtained from 13 samples in four different experiments, and error bars indicate standard deviations from the mean. *: At the 0.05 level, there is significant difference between the control and the N-GQDs or GO -treated RBCs.

SEIRAS studies of the interaction between GO or N-GQDs and RBC membranes using model membranes

Since the cause of cytotoxicity is related to how nanomaterials interact with cell membranes,[40] we employed SEIRAS to investigate the GO or N-GQDs-induced structural changes in model membranes prepared on solid supports with lipid compositions identical to those of RBC membranes. As in the previous study, we prepared the model membranes respectively with three lipid components that were identical to the compositions in the outer or inner lipid leaflet of RBC membranes. The planar membrane was formed by vesicle fusion on the hydrophobic surface of a pre-adsorbed 1-dodecanethiol (DT) monolayer on a gold film.[42] A spectrum of the planar membrane with lipid components of the outer leaflet is shown in the upper panel of Fig. 5A (a) and S3.† The bands at 2928 and 2854 cm^{-1} are attributed to the asymmetric, $\nu_{as}(CH_2)$, and symmetric, $\nu_s(CH_2)$, stretching vibrations of methylene, and the bands at 2959 and 2870 cm^{-1} are assigned to the asymmetric, $\nu_{as}(CH_3)$, and symmetric, $\nu_s(CH_3)$, stretching vibrations of the methyl group, respectively. In the fingerprint region, the spectrum of the outer leaflet shows the C═O stretching vibration of lipid at 1741 cm^{-1},[46] with a strong negative peak at 1656 cm^{-1}, which is associated with the OH bending vibration of water, because of the highly hydrophobic environment in the lipid bilayer.[42] The band at 1280 cm^{-1} is due to the twist vibration of the polymethylene chains of lipid.[63] After the formation of the planar membrane, the substrate was washed several times with distilled water to remove the free vesicles. The spectrum of the membrane-modified substrate immersed in water was taken as the reference, and 50 μg mL^{-1} of GO or N-GQDs was added before recording the sample spectra. When GO interacted with the model membrane, obvious negative peaks were induced at the $\nu_{as}(CH_3)$ and $\nu_s(CH_3)$ positions, accompanied by the disappearance of absorptions at the $\nu_{as}(CH_2)$, and $\nu_s(CH_2)$ vibrations (Fig. 5A, b and S4†), which were observed in the SEIRA spectrum of the control GO (Fig. 5B, a). According to the report of Huang and Zhou *et al.*, GO nanosheets can insert/cut the membrane and extract large amounts of phospholipids from the cellular membranes driven by strong van der Waals force.[40] During the interaction of GO with the model membrane, extraction of lipid might occur due to the strong hydrophobic nature of the outer lipid leaflet, and result in negative peaks at the CH_3 and CH_2 vibration positions. Meanwhile, peaks at the $\nu_{as}(CH_2)$ and $\nu_s(CH_2)$ positions can be observed for the adsorbed GO as shown in the SEIRA spectrum of control GO (Fig. 5B, a), which compensates for the negative peaks at these positions which are induced by lipid extraction. That is why we only observed the disappearance of the peaks at the $\nu_{as}(CH_3)$ and $\nu_s(CH_3)$

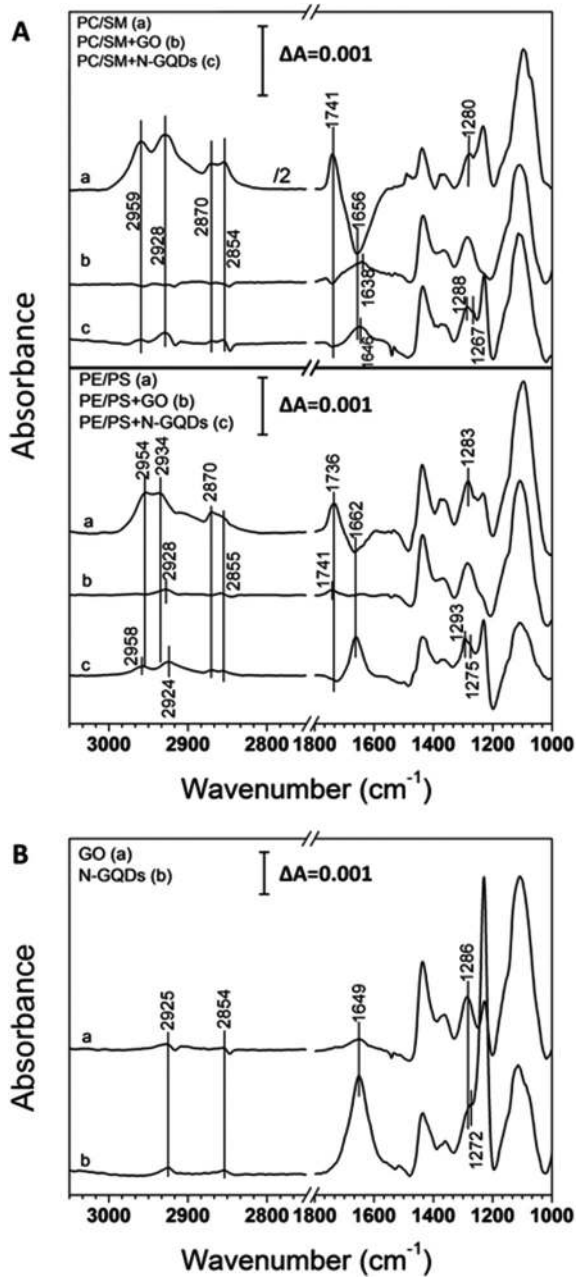

Fig. 5 (A) SEIRA spectra of vesicles containing the lipids of the outer (upper panel) and inner (lower panel) lipid leaflet of RBCs adsorbed on DT-modified gold (a), and the GO (b) or N-GQDs (c) adsorbed on the lipid/DT modified gold surface. (B) SEIRA spectra of control GO (a) and N-GQDs (b).

vibration. In the fingerprint region, the negative peak at 1741 cm^{-1} assigned to C═O confirmed the extraction of lipid. In addition, we also observed that the vibration of C═C in GO was shifted from 1649 cm^{-1} to 1638 cm^{-1} (Fig. 5B, a).[64–66] During the extraction of lipid, the hydrophobic tails of lipid tended to spread out in the unoxidized hydrophobic regions of GO.[40] As a result, the strong interaction between GO and lipid might influence the skeleton structure of the aromatic rings in GO, and induce the shift of the vibration of C═C. When GQDs interacted with the model membrane, new peaks appeared at the $\nu_{as}(CH_3)$ and $\nu_s(CH_3)$ position (Fig. 5A, c and S5†), which were not observed in the control spectrum of GQDs (Fig. 5B, b). The appearance of the new peaks at CH_3 vibrations suggests interaction of the N-GQDs with the CH_3 group in the lipid model membrane. But N-GQDs couldn't induce extraction of lipid, because there were two obvious positive peaks at the CH_2 vibrations in the difference spectrum induced by adsorption of N-GQDs. In the fingerprint region, the band at 1649 cm^{-1} was slightly shifted to 1646 cm^{-1} after N-GQDs interacted with the lipid membranes. The strong peaks at 1649 cm^{-1} in the control N-GQDs spectrum should be assigned to the acidamide (-CO-NR_2), accompanied by the vibration of the skeletal aromatic rings in N-GQDs.[64–66] The slight shift suggests that the interaction between N-GQDs and lipid did not exert an obvious influence on the structure of N-GQDs. It is worth noting that the interaction of N-GQDs induced the peak shift of the twist vibration of polymethylene chains of lipid from 1280 cm^{-1} to 1288 cm^{-1}, and a shoulder peak at 1267 cm^{-1}, suggesting that the interaction of N-GQDs induced obvious disturbance in the conformers of lipid.

According to the molecular dynamics simulations in Huang and Zhao' report, graphene or GO could insert/cut into a membrane,[40] so the inner leaflet of RBC membranes would also be influenced. Likewise, we also studied the interaction of GO and N-GQDs using a model membrane composed of the lipid compositions of the inner leaflet of RBC membranes. The spectrum of the model membrane is shown in the lower panel of Fig. 5A and S6.† Due to the overlap with $\nu_{as}(CH_3)$ and $\nu_s(CH_3)$ respectively, the bands assigned to $\nu_{as}(CH_2)$ and $\nu_s(CH_2)$ were broader in comparison with the spectrum of the outer lipid layer (upper panel, a). The C═O stretching was observed at 1736 cm^{-1}, with a much weaker negative peak at 1662 cm^{-1} in comparison with that in the outer membrane at 1656 cm^{-1}, indicating a less hydrophobic inner microenvironment.[42] Similar to the outer membrane, twist vibration of the polymethylene chains of the inner lipid was observed at 1283 cm^{-1}. In the GO-induced SEIRA difference spectrum (Fig. 5A, lower panel, b and S7†), the bands at 2928 cm^{-1} and 2855 cm^{-1} are visible, which are due to the $\nu_{as}(CH_2)$ and $\nu_s(CH_2)$ of GO (Fig. 5B, a), respectively. But no obvious negative peak was observed in the CH region, suggesting that GO could not induce the extraction of the inner leaflet lipids. Extraction was driven by the strong hydrophobic interaction between the GO nanosheet and membrane lipid.[40] The much weaker hydrophobicity of the inner leaflet lipid might not be enough to form a strong interaction with GO and induce lipid extraction. In the fingerprint region, GO induced a slight peak at 1741 cm^{-1}, which is assigned to C═O stretching and not observed in the SEIRA spectrum of GO (Fig. 5B, a), suggesting interaction of GO with the ester carbonyl/carboxylate group in the inner leaflet lipid. In the GQDs-induced SEIRA difference spectrum (Fig. 5A, lower panel, c and S8†), beside the bands of $\nu_{as}(CH_2)$ and $\nu_s(CH_2)$ at 2924 and 2855 cm^{-1} that might derive from the vibrations of adsorbed N-GQDs, we also observed additional vibrations due to $\nu_{as}(CH_3)$ and $\nu_s(CH_3)$, which were

not observed in the spectrum of N-GQDs (Fig. 5B, b). Moreover, the vibration of $\nu_{as}(CH_3)$ was blue shifted in comparison with the position of $\nu_{as}(CH_3)$ in the lipid. These indicate interaction of N-GQDs with the alkyl groups of the inner leaflet lipid. A strong peak at 1662 cm^{-1} accompanied by a peak shift from 1649 cm^{-1} in comparison with the SEIRA spectrum of N-GQDs (Fig. 5B, b) suggests a strong interaction between GQDs and the inner lipid. Since the hydrophilicity of the inner lipid membrane is much stronger than that of the outer lipid membrane, when N-GQDs were added to the surface of the inner membrane, the strong hydrophilic interaction might change the vibration mode of the bond in N-GQDs. Besides, in the difference spectrum, the peak of the twist vibration of polymethylene chains of lipid shifted from 1283 cm^{-1} to 1293 cm^{-1} with a shoulder at 1275 cm^{-1}, suggesting that the interaction of N-GQDs with alkyl group in the inner lipid disturbed the conformations of lipid.

To gain a further understanding of the process of interaction between the graphene forms and model membrane, we investigated the dynamics by integrating the area of the peak at around 1095 cm^{-1} during the incubation of the model membrane with the graphene forms and analyzed the change with time. The data was fitted according to the exponential function as shown in Fig. 6, which yields a good agreement between the experimental (symbol) and simulated (line) data with a residual square correlation coefficient ($R^2 > 0.99$). According to the fitted curves, the half-times of GO interacting with the outer and inner lipids were 31 and 9 min, and that of N-GQDs interacting with the outer and inner lipids were 7 and 11 min, respectively.

Obviously, the half-time of GO interaction with the outer lipid was much longer than the others. The different dynamics might come from the difference of the acting force between the model membranes and graphene materials. When GO interacted with the outer model membrane, the hydrophobic interaction between the outer lipid and the GO resulted in a longer time in achieving an interactional equilibrium. For the hydrophilic interaction, the process could achieve equilibrium in a shorter time.

Combining the results obtained by SEIRAS, we could conclude that the hemolysis and morphological variations of RBCs induced by GO and N-GQDs were mostly related to the types of interactions between the graphene materials and the RBC membranes. The microenvironment in the outer leaflet lipid of RBCs was more hydrophobic than that in the inner leaflet lipid. Such a difference determined the different interaction modes between the lipid and graphene forms. GO had the strong hydrophobic interaction with the outer lipid, resulting in the extraction of the outer lipid and a longer time in achieving adsorption equilibrium. The extraction broke the integrity of the outer membrane, although there was a weak interaction with the inner lipid, and eventually resulted in hemolysis. N-GQDs had strong hydrophilic interaction with the inner lipid, and weak interaction with the outer lipid. Adsorption of N-GQDs on both leaflet lipids achieved equilibrium in a short time, and only disturbed the conformation of the lipid. It has been reported that partition of some drugs into the membranes of RBCs generated echinocytes.[67] Due to their small size, N-GQDs might be incorporated into the lipid of RBC membranes, and result in the formation of echinocytes. As a result, N-GQDs would just induce some morphological variations, but wouldn't break the integrity of the membrane and induce hemolysis. According to Haynes's report, above 342 nm, the smaller GO showed a greater hemolytic activity.[27] According to our results and the previously reported results, there might be a critical size that keeps the balance between hydrophobicity and hydrophilicity. When the size of graphene materials is larger than the critical value, the hydrophobicity is the decisive factor that induces lipid extraction. When the size of the graphene materials is smaller than the critical value, the size might be the key factor that induces disturbance of the RBC membrane. This might be an interesting issue for future study.

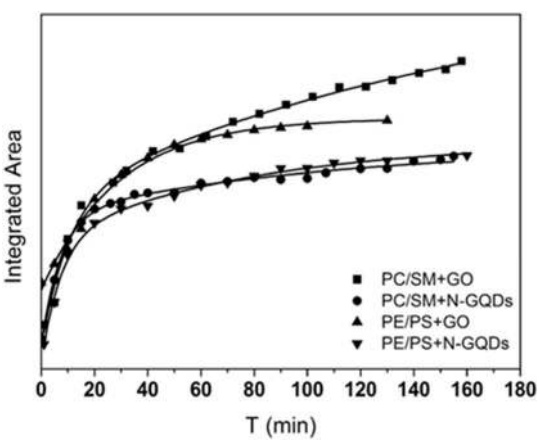

Fig. 6 The dynamics curves of the interaction of the outer model lipids with GO (■) or N-GQDs (●), and the inner model lipids with GO (▲) or N-GQDs (▼). Integrated area of the peak at around 1095 cm^{-1} was plotted as a function of time.

Conclusions

In summary, we have systematically studied the toxicity of two typical graphene forms, GO and N-GQDs, in RBCs. The toxicity was evaluated by detecting their hemolytic activity using UV-visible spectroscopy, and observing the shape changes of RBCs by confocal microscopy. The ATP content in RBCs was also detected to explore the reasons for the shape changes. The results indicated that GO induced obvious hemolysis of RBCs, accompanied by the release of ATP. Correspondingly, lots of ghost and aberrant cells were observed. In comparison with GO, N-GQDs did not induce any hemolysis and an obvious release of ATP from RBCs. However, lots of echinocytes were observed unexpectedly. For an in-depth understanding of the mechanism of the cytotoxicity, SEIRAS was further applied in the study of the interaction of graphene nanomaterials with RBC membranes using solid-supported model membranes

prepared with identical lipid compositions to those of RBC membranes. Our results suggested that GO was adsorbed onto the lipid bilayer of RBCs *via* strong hydrophobic interaction and extracted the lipid. Hemolysis was induced by the destruction of the RBCs membrane integrity, and the aberrant forms might be induced by structural change of the lipid together with the release of ATP in RBCs. Whereas N-GQDs just disturbed the order and conformation of lipid, which might be induced by the incorporation of small N-GQDs into the lipid, resulting in the formation of echinocytes. Our study suggested that although graphene forms have exhibited outstanding properties in biological and biomedical applications, the toxicity of these materials should be under consideration all the time, especially in the circulatory system.

Experimental section

Synthesis and characterization of GO and N-GQDs

Graphene oxide (GO) was synthesized *via* a modified Hummer's method from natural graphite powder.[51,52] In a typical synthesis, 1 g of graphite powder was added into 23 mL of 98% H_2SO_4 in a round flask, followed by stirring at room temperature over 24 h. After that, 100 mg of $NaNO_3$ was added under stirring and kept stirring for 30 min. Then, the mixture was cooled down to below 5 °C in an ice bath, and 3 g of $KMnO_4$ was added slowly. The mixture was heated to about 35 °C and stirred for another 30 min. After that, 46 mL of H_2O was slowly added in three separate doses (5, 10, 31 mL in sequence) within 25 min and the mixture was continually heated until the temperature reach 98 °C and kept refluxing for 20 min. Finally, 27.5 mL of water and 3.5 mL of 30% H_2O_2 were added into the mixture to stop the reaction. The obtained graphite oxide should be washed with water until neutral, and exfoliated by ultrasonication using a bath-sonicator (KQ-200KDE, 200 W, Kunshan, China) for about 5 h. The solid GO was obtained by freeze-drying or vacuum drying at 45 °C.

Nitrogen-doped graphene quantum dots (N-GQDs) were prepared according to a previous report.[23] In brief, 150 mg of the obtained GO was dissolved in 15 mL of dimethylformamide (DMF) at a concentration of 10 mg ml^{-1}. After ultrasonication for 30 min, the mixture was transferred into a poly(tetrafluoroethylene) (Teflon)-lined autoclave (30 mL), followed by heating at 200 °C for 5 h. After the reaction, the reactor was cooled to room temperature naturally. The brown transparent suspension was collected by filtering the product with filter membrane (0.45 μm, Shanghai Xingya, China) to discard the black precipitates. The solid N-GQD samples were obtained by removing the solvents with the aid of a rotary evaporator.

X-ray photoelectron spectroscopy (XPS) of the as-prepared GO and N-GQDs was carried out using an ESCALAB 250 spectrometer with a mono X-Ray source AlKα excitation (1486.6 eV). The C1s spectra of XPS were fitted and decomposed using XPSPEAK41 software. The morphologies of the N-GQDs and GO were characterized by transmission electron microscopy (TEM) measurements using an Hitachi H-800 electron microscope at an acceleration voltage of 200 kV with a CCD cinema and an Hitachi H-8100 electron microscope (Hitachi, Tokyo, Japan), respectively.

Hemolysis assay

Human blood was freshly collected from healthy adult volunteers in the Hospital of Integrated Traditional and Western Medicine in Jilin province. RBCs were separated by centrifuging the whole blood at 10 016*g* for 10 min and washing five times with sterile phosphate buffered saline (PBS). 0.2 mL of packed RBCs was diluted to 3 mL with PBS as stock solution. Then 0.2 mL of the diluted RBCs suspension was taken out and mixed with 0.8 mL of GO or N-GQDs solution in PBS at systematically varied concentrations (3.1, 6.2, 12.5, 25, 50, 100, 200 μg mL^{-1}). The GO and N-GQDs solutions of different concentrations were prepared immediately before dilution of the RBCs. For preparing negative and positive control samples, we mixed 0.2 mL of RBCs suspension with 0.8 mL of PBS and water respectively, instead of GO and N-GQDs solutions. After that, all the samples were incubated in a humidified incubator at 37 °C, 5% CO_2 for 3 h, and finally centrifuged at 10 016*g* for 3 min. 800 μL of the supernatant of all the samples were taken out for UV-visible measurements. The percent of RBCs hemolysis was calculated using the following formula: hemolysis % = ((sample absorbance − negative control absorbance)/(positive control absorbance − negative control absorbance)) × 100. In the formula, the absorbance value of the hemoglobin at 541 nm was used with the reference wavelength at 650 nm.

Cellular images

In this section, we chose the RBCs that were treated with 50 μg mL^{-1} of GO or N-GQDs for imaging. All the procedures were the same as that for the hemolysis assay. Just after centrifugation, the sediment RBCs were washed 3 times with PBS and resuspended in 2 mL of PBS. Then 0.7 mL of the suspension was injected into a 35 mm tissue culture dish (NEST Biotech Co., LTD., China), and the dishes were left at room temperature in a static state for 20 min to allow the cells to attach to the bottom of the glass slide. After that, the cells were washed 3 times with PBS to remove the unattached cells. The images of the cells were taken using a confocal laser scanning fluorescence microscope (CLSM, Leica TCS SP2, Leica Microsystems, Mannheim, Germany) with 100× objective in the bright field.

ATP detection assay

Before detection, RBCs were treated with 50 μg mL^{-1} of GO or N-GQDs as for the hemolysis assay, and all of the solutions (including lysate, detecting regent and corresponding diluent) in the ATP assay kit (Beyotime, China) were defrosted at 4 °C in advance, and placed on ice for use. After incubation with GO or N-GQDs solutions for 3 h, the samples were centrifuged at 10 016*g* for 3 min, followed by discarding the suspension. The sediment cells were lysed by adding 120 μL of lysate to release the ATP in the cells. The working solution was prepared by diluting the detecting regent with corresponding diluent at a ratio of 1 : 100 and kept in the dark on ice. 100 μL of working

solution per well were injected into a 96-well plate and the plate was kept in the dark for 5 min to consume the background. Then, 100 μL of the lysed cells were added and mixed with the working solution quickly, immediately followed by measurement using a Synergy HT Multi-Mode Microplate Reader (Biotek, US) with Gen5 data analysis software. 13 samples were collected from four repeated experiments for each set of data.

In situ surface-enhanced infrared absorption spectroscopy (SEIRAS)

The experimental setup for SEIRAS and procedures for preparation of Au film as enhanced substrate have been described elsewhere.[42,46,48,68] Briefly, a thin gold film was deposited on the flat surface of a triangular silicon prism by a chemical deposition technique. The surface of the Si prism was polished with aluminum oxide powder of 1 μm in size, followed by immersion in a 40 wt% aqueous solution of NH_4F for 1 min. Subsequently, the flat surface of the Si prism was exposed to a 1 : 1 : 1 volume mixture of (1) 0.03 M $NaAuCl_4$, (2) 0.3 M Na_2SO_4 + 0.1 M $Na_2S_2O_3$ + 0.1 M NH_4Cl, and (3) 2.5 vol% HF solution for about 1 min. After rinsing several times with water, the gold film was cleaned in 0.1 M H_2SO_4 by carrying out several electrochemical cycles. Subsequently, the gold-coated prism was mounted into a polytrifluorochloroethylene cell. The IR beam of the FTIR spectrometer (IFS 66 s/v, Bruker, Ettlingen, Germany) was coupled into the silicon prism at an incident angle of 60°, and the spectra were recorded with a liquid-nitrogen-cooled MCT detector. The Au film was immersed in 1 mM of 1-dodecanethiol (DT, Sigma-Aldrich) that was dissolved in ethanol for 30 min. During this time, the spectra were recorded every 2 min with pure ethanol as the reference. After the film was washed with ethanol and water three times, respectively, 200 μL of double distilled water was added and the spectrum was recorded as the background. After adding 1 mL of the vesicle solution, the signals were recorded as sample spectra every 3 min during the subsequent 2–3 h. Before the next step, the substrate was washed sufficiently with water. Then the model lipid was immersed in 50 μg mL^{-1} of GO or N-GQDs aqueous solution for incubation. Simultaneously, the sample spectra were recorded every 1 minute during the first 30 minutes with double distilled water as the reference. And then, the signals were recorded every 3 minutes during the subsequent 2–3 h. As the control experiment, we also measured the spectra of GO and N-GQDs by adding 50 μg mL^{-1} of GO or N-GQDs aqueous solution to the Au film with water as the reference. For each spectrum, 512 scans were collected with a spectrum resolution of 4 cm^{-1}. Every experiment was repeated at least 3 times. More than sixty spectra were collected from three repeated experiments at the last hour for every step, and were averaged to reduce the background.

Preparation of vesicles

Egg phosphatidylcholine (PC), sphingomyelin (SM), and cholesterol (Sigma-Aldrich, St. Louis, MO) were mixed at a ratio of 1 : 1 : 1 (by weight); dioleoyl phosphoethanolamine (DOPE), dioleoyl phosphatidylserine (DOPS), and cholesterol (Sigma-Aldrich) were mixed at a ratio of 2 : 1 : 1 (by weight). The mixtures were dissolved in chloroform in two little glass bottles respectively, and the solvent was removed by rotary evaporation under N_2 flow to form a thin lipid layer. In order to get rid of the chloroform thoroughly, the bottles were kept in a vacuum chamber for 3 h. Double distilled water was added to hydrate the dried lipid film for 30 min and yield a final concentration of 1 mg mL^{-1}. Then sonication was performed at 40 °C to yield a clear solution. The vesicles were always used within 24 h after preparation.

All of the experiments were performed in compliance with the relevant laws and guidelines of Changchun Institute of Applied Chemistry. The institutional committee of *in vivo* experiment has approved the experiments and informed consent was obtained for any experimentation with human subjects.

Acknowledgements

This work was supported by the National Science Foundation of China (grants 21322510, 21105097, and 91227114), the Natural Science Foundation of Jilin Province (201215092) and President Funds of the Chinese Academy of Sciences.

Notes and references

1 A. Albanese, P. S. Tang and W. C. W. Chan, *Annu. Rev. Biomed. Eng.*, 2012, **14**, 1–16.
2 J. Blechinger, A. T. Bauer, A. A. Torrano, C. Gorzelanny, C. Bräuchle and S. W. Schneider, *Small*, 2013, **9**, 3970–3980.
3 Y. Chang, S.-T. Yang, J.-H. Liu, E. Dong, Y. Wang, A. Cao, Y. Liu and H. Wang, *Toxicol. Lett.*, 2011, **200**, 201–210.
4 J. M. Dowding, S. Das, A. Kumar, T. Dosani, R. McCormack, A. Gupta, T. X. T. Sayle, D. C. Sayle, L. von Kalm, S. Seal and W. T. Self, *ACS Nano*, 2013, **7**, 4855–4868.
5 S.-Q. Li, R.-R. Zhu, H. Zhu, M. Xue, X.-Y. Sun, S.-D. Yao and S.-L. Wang, *Food Chem. Toxicol.*, 2008, **46**, 3626–3631.
6 J. Q. Lin, H. W. Zhang, Z. Chen and Y. G. Zheng, *ACS Nano*, 2010, **4**, 5421–5429.
7 L. Peng, M. He, B. Chen, Q. Wu, Z. Zhang, D. Pang, Y. Zhu and B. Hu, *Biomaterials*, 2013, **34**, 9545–9558.
8 D. Li and R. B. Kaner, *Science*, 2008, **320**, 1170–1171.
9 K. S. Novoselov, A. K. Geim, S. V. Morozov, D. Jiang, Y. Zhang, S. V. Dubonos, I. V. Grigorieva and A. A. Firsov, *Science*, 2004, **306**, 666–669.
10 S. Park and R. S. Ruoff, *Nat. Nanotechnol.*, 2009, **4**, 217–224.
11 C. N. R. Rao, A. K. Sood, K. S. Subrahmanyam and A. Govindaraj, *Angew. Chem., Int. Ed.*, 2009, **48**, 7752–7777.
12 D. R. Dreyer, S. Park, C. W. Bielawski and R. S. Ruoff, *Chem. Soc. Rev.*, 2010, **39**, 228–240.

13 S. Stankovich, D. A. Dikin, R. D. Piner, K. A. Kohlhaas, A. Kleinhammes, Y. Jia, Y. Wu, S. T. Nguyen and R. S. Ruoff, *Carbon*, 2007, **45**, 1558–1565.
14 Y. Tao, Y. Lin, Z. Huang, J. Ren and X. Qu, *Adv. Mater.*, 2013, **25**, 2594–2599.
15 Y. Wang, Z. Li, D. Hu, C.-T. Lin, J. Li and Y. Lin, *J. Am. Chem. Soc.*, 2010, **132**, 9274–9276.
16 A. K. Geim, *Science*, 2009, **324**, 1530–1534.
17 S. Stankovich, D. A. Dikin, G. H. B. Dommett, K. M. Kohlhaas, E. J. Zimney, E. A. Stach, R. D. Piner, S. T. Nguyen and R. S. Ruoff, *Nature*, 2006, **442**, 282–286.
18 H. Zhang, Y. Sun, S. Gao, J. Zhang, H. Zhang and D. Song, *Small*, 2013, **9**, 2537–2540.
19 E. Morales-Narváez and A. Merkoçi, *Adv. Mater.*, 2012, **24**, 3298–3308.
20 X. Sun, Z. Liu, K. Welsher, J. Robinson, A. Goodwin, S. Zaric and H. Dai, *Nano Res.*, 2008, **1**, 203–212.
21 Z. Liu, J. T. Robinson, X. Sun and H. Dai, *J. Am. Chem. Soc.*, 2008, **130**, 10876–10877.
22 L.-L. Li, J. Ji, R. Fei, C.-Z. Wang, Q. Lu, J.-R. Zhang, L.-P. Jiang and J.-J. Zhu, *Adv. Funct. Mater.*, 2012, **22**, 2971–2979.
23 S. Zhu, J. Zhang, C. Qiao, S. Tang, Y. Li, W. Yuan, B. Li, L. Tian, F. Liu, R. Hu, H. Gao, H. Wei, H. Zhang, H. Sun and B. Yang, *Chem. Commun.*, 2011, **47**, 6858–6860.
24 H. Bao, Y. Pan, Y. Ping, N. G. Sahoo, T. Wu, L. Li, J. Li and L. H. Gan, *Small*, 2011, **7**, 1569–1578.
25 W. H. Kong, D. K. Sung, K. S. Kim, H. S. Jung, E. J. Gho, S. H. Yun and S. K. Hahn, *Biomaterials*, 2012, **33**, 7556–7564.
26 Z. Tang, H. Wu, J. R. Cort, G. W. Buchko, Y. Zhang, Y. Shao, I. A. Aksay, J. Liu and Y. Lin, *Small*, 2010, **6**, 1205–1209.
27 K.-H. Liao, Y.-S. Lin, C. W. Macosko and C. L. Haynes, *ACS Appl. Mater. Interfaces*, 2011, **3**, 2607–2615.
28 M. Nurunnabi, Z. Khatun, K. M. Huh, S. Y. Park, D. Y. Lee, K. J. Cho and Y.-k. Lee, *ACS Nano*, 2013, **7**, 6858–6867.
29 S. K. Singh, M. K. Singh, P. P. Kulkarni, V. K. Sonkar, J. J. A. Grácio and D. Dash, *ACS Nano*, 2012, **6**, 2731–2740.
30 K. Wang, J. Ruan, H. Song, J. Zhang, Y. Wo, S. Guo and D. Cui, *Nanoscale Res. Lett.*, 2011, **6**, 8.
31 H. Zhang, C. Peng, J. Yang, M. Lv, R. Liu, D. He, C. Fan and Q. Huang, *ACS Appl. Mater. Interfaces*, 2013, **5**, 1761–1767.
32 N. Abdullah Al, J.-E. Lee, I. In, H. Lee, K. D. Lee, J. H. Jeong and S. Y. Park, *Mol. Pharmaceutics*, 2013, **10**, 3736–3744.
33 Q. Liu, B. Guo, Z. Rao, B. Zhang and J. R. Gong, *Nano Lett.*, 2013, **13**, 2436–2441.
34 M. Nurunnabi, Z. Khatun, M. Nafiujjaman, D.-g. Lee and Y.-k. Lee, *ACS Appl. Mater. Interfaces*, 2013, **5**, 8246–8253.
35 Y. Chong, Y. Ma, H. Shen, X. Tu, X. Zhou, J. Xu, J. Dai, S. Fan and Z. Zhang, *Biomaterials*, 2014, **35**, 5041–5048.
36 W. Shang, X. Zhang, M. Zhang, Z. Fan, Y. Sun, M. Han and L. Fan, *Nanoscale*, 2014, **6**, 5799–5806.
37 C. Wu, C. Wang, T. Han, X. Zhou, S. Guo and J. Zhang, *Adv. Healthcare Mater.*, 2013, **2**, 1613–1619.
38 Y. Zhao, Q. Liu, S. Shakoor, J. R. Gong and D. Wang, *Toxicol. Res.*, 2015, DOI: 10.1039/C4TX00123K.
39 R. F. Service, *Science*, 2004, **304**, 1732–1734.
40 Y. Tu, M. Lv, P. Xiu, T. Huynh, M. Zhang, M. Castelli, Z. Liu, Q. Huang, C. Fan, H. Fang and R. Zhou, *Nat. Nanotechnol.*, 2013, **8**, 594–601.
41 J. Heberle and K. Ataka, in *Encyclopedia of Biophysics*, ed. G. K. Roberts, Springer, Berlin Heidelberg, 2013, pp. 2528–2531.
42 T. Wang, J. Bai, X. Jiang and G. U. Nienhaus, *ACS Nano*, 2012, **6**, 1251–1259.
43 J. Li, R. Strong, J. Trevisan, S. W. Fogarty, N. J. Fullwood, K. C. Jones and F. L. Martin, *Environ. Sci. Technol.*, 2013, **47**, 10005–10011.
44 M. J. Riding, F. L. Martin, J. Trevisan, V. Llabjani, I. I. Patel, K. C. Jones and K. T. Semple, *Environ. Pollut.*, 2012, **163**, 226–234.
45 M. J. Riding, J. Trevisan, C. J. Hirschmugl, K. C. Jones, K. T. Semple and F. L. Martin, *Environ. Int.*, 2012, **50**, 56–65.
46 K. Ataka, F. Giess, W. Knoll, R. Naumann, S. Haber-Pohlmeier, B. Richter and J. Heberle, *J. Am. Chem. Soc.*, 2004, **126**, 16199–16206.
47 J. Kozuch, C. Steinem, P. Hildebrandt and D. Millo, *Angew. Chem., Int. Ed.*, 2012, **51**, 8114–8117.
48 K. Ataka and J. Heberle, *J. Am. Chem. Soc.*, 2004, **126**, 9445–9457.
49 X. Jiang, M. Engelhard, K. Ataka and J. Heberle, *J. Am. Chem. Soc.*, 2010, **132**, 10808–10815.
50 X. Jiang, E. Zaitseva, M. Schmidt, F. Siebert, M. Engelhard, R. Schlesinger, K. Ataka, R. Vogel and J. Heberle, *Proc. Natl. Acad. Sci. U. S. A.*, 2008, **105**, 12113–12117.
51 W. S. Hummers and R. E. Offeman, *J. Am. Chem. Soc.*, 1958, **80**, 1339–1339.
52 W. Lu, R. Ning, X. Qin, Y. Zhang, G. Chang, S. Liu, Y. Luo and X. Sun, *J. Hazard. Mater.*, 2011, **197**, 320–326.
53 L.-Y. Meng and S.-J. Park, *Bull. Korean Chem. Soc.*, 2012, **33**, 209–214.
54 J. Shang, L. Ma, J. Li, W. Ai, T. Yu and G. G. Gurzadyan, *Sci. Rep.*, 2012, **2**, 792.
55 J. Zhang, H. Yang, G. Shen, P. Cheng, J. Zhang and S. Guo, *Chem. Commun.*, 2010, **46**, 1112–1114.
56 P. V. Asharani, S. Sethu, S. Vadukumpully, S. Zhong, C. T. Lim, M. P. Hande and S. Valiyaveettil, *Adv. Funct. Mater.*, 2010, **20**, 1233–1242.
57 L. Backman, *J. Cell Sci.*, 1986, **80**, 281–298.
58 A. V. Gourine, E. Llaudet, N. Dale and K. M. Spyer, *Nature*, 2005, **436**, 108–111.
59 M. Nakao, T. Nakao and S. Yamazoe, *Nature*, 1960, **187**, 945–946.
60 M. Nakao, S. Yamazoe, H. Yoshikawa and T. Nakao, *J. Biochem.*, 1961, **49**, 487–492.
61 N. Mohandas and S. B. Shohet, *Curr. Top. Hematol.*, 1978, **1**, 71–125.
62 R. I. Weed, P. L. Lacelle and E. W. Merrill, *J. Clin. Invest.*, 1969, **48**, 795–809.
63 D. Chapman, *J. Am. Oil Chem. Soc.*, 1965, **42**, 353–371.

64 F. Y. Ban, S. R. Majid, N. M. Huang and H. N. Lim, *Int. J. Electrochem. Sci.*, 2012, **7**, 4345–4351.
65 M. Hilder, O. Winther-Jensen, B. Winther-Jensen and D. R. MacFarlane, *Phys. Chem. Chem. Phys.*, 2012, **14**, 14034–14040.
66 H. Zhang, D. Hines and D. L. Akins, *Dalton Trans.*, 2014, **43**, 2670–2675.
67 W. B. Gratzer, *Biochem. J.*, 1981, **198**, 1–8.
68 K. Ataka and J. Heberle, *J. Am. Chem. Soc.*, 2003, **125**, 4986–4987.